Supporting information for

Computational Insights into the Interaction of Water with the UiO-66 Metal-organic Framework and Its Functionalized Derivatives

Jierui Zhang[a], *Francesco Paesani*[b]*, *Martina Lessio*[a]*

[a] School of Chemistry, The University of New South Wales, Sydney, NSW 2052, Australia

[b] Department of Chemistry and Biochemistry, University of California San Diego, La Jolla, CA, United States.

1. Bonded force field parameters derivation and benchmark

1.1. Cluster model for density functional theory calculations

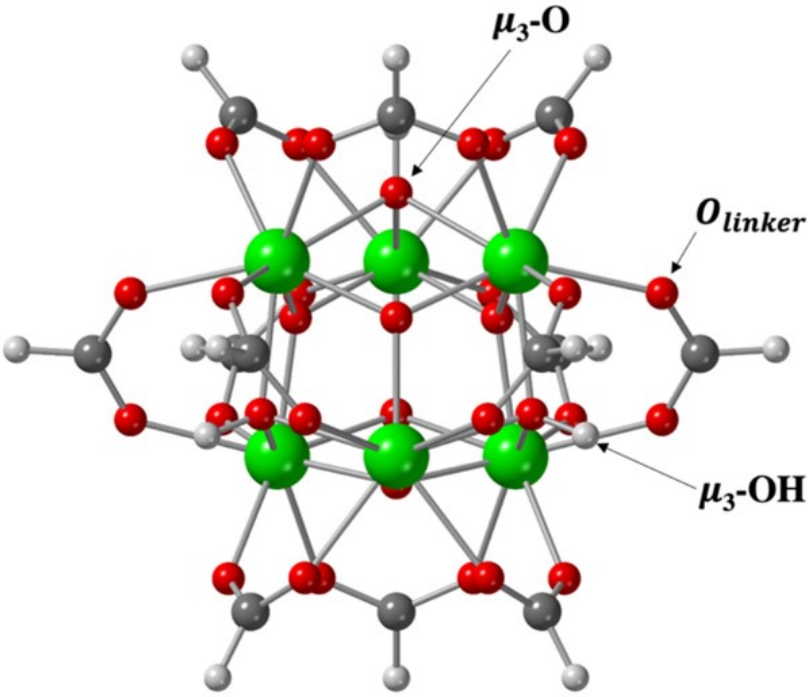

Figure S1: UiO-66 cluster model generated by truncating the periodic structure. Arrows and labels indicate the three interaction sites for water. Zr atoms are represented by green spheres, O atoms by red spheres, C atoms by grey spheres, and H atoms by white spheres.

1.2. Benchmarking of bonded force field parameters

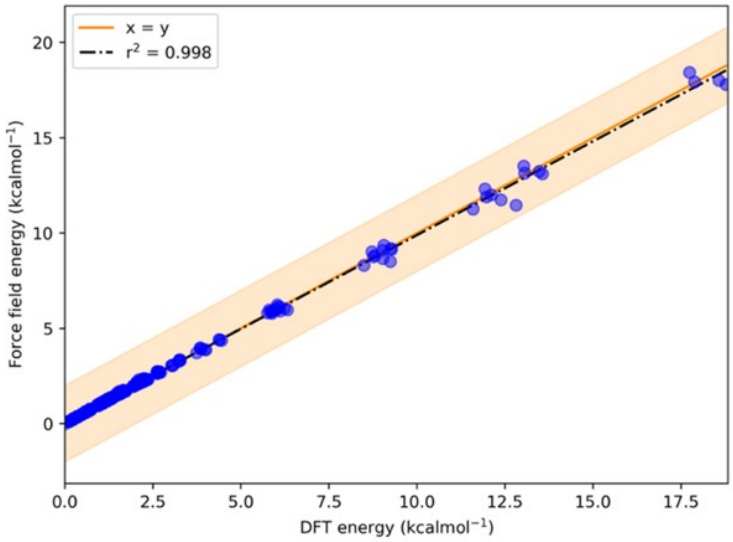

Figure S2: Correlation curve between energies calculated with our classical force field and DFT energies for the UiO-66 cluster model.

The correlation between the DFT energies and the derived force field energies for the UiO-66 cluster model is shown in Figure S2. We find that the derived force field model can successfully reproduce the DFT energies (linear correlation coefficient $R^2 = 0.998$). As seen in Figure S2, the majority of the geometries considered in the fitting process have low relative energies corresponding to minor distortions of the equilibrium structure, with only a few strongly distorted high energy geometries. This is a valid approach since the rigidity of the metal-organic framework (MOF) framework limits the vibrational freedom of the atoms within the lattice.

Table S1: The unit cell parameter and relevant bond distances in the metal node of UiO-66 calculated through molecular dynamic (MD) and from experimental crystallographic data.[1] All results are reported in Angstrom.

Parameters	**This work (MD simulation)**	**Experimental crystallographic data**[1]
$a = b = c$	20.7694	20.7465
Zr-O_{linker}	2.241	2.214
Zr-μ_3-O	2.112	2.062
Zr-μ_3-OH	2.166	2.258
O-OH (μ_3-OH)	0.987	0.607

The force filed employed to model the MOFs is a combination of parameters for the inorganic units developed in this work and parameters for the organic linkers obtained from the General Amber Force Fields (GAFF).[2] It is therefore important to ensure that this combined force field correctly reproduces unit cell parameters and relevant bond lengths from experimental crystallographic data.[1] For this purpose, we equilibrated the UiO-66 unit cell through a constant pressure and constant temperature (*NPT*) canonical ensemble simulation for 1 ns, at 1 atm and 100 K since the experimental crystallographic results are measured under these conditions.[1] The unit cell parameters and bond distances (Table S1) were then obtained

by averaging across a 1 ns *NPT* production trajectory. As shown in Table S1, the cell parameters and the bond distances in the metal node closely match the experimental data.[1]

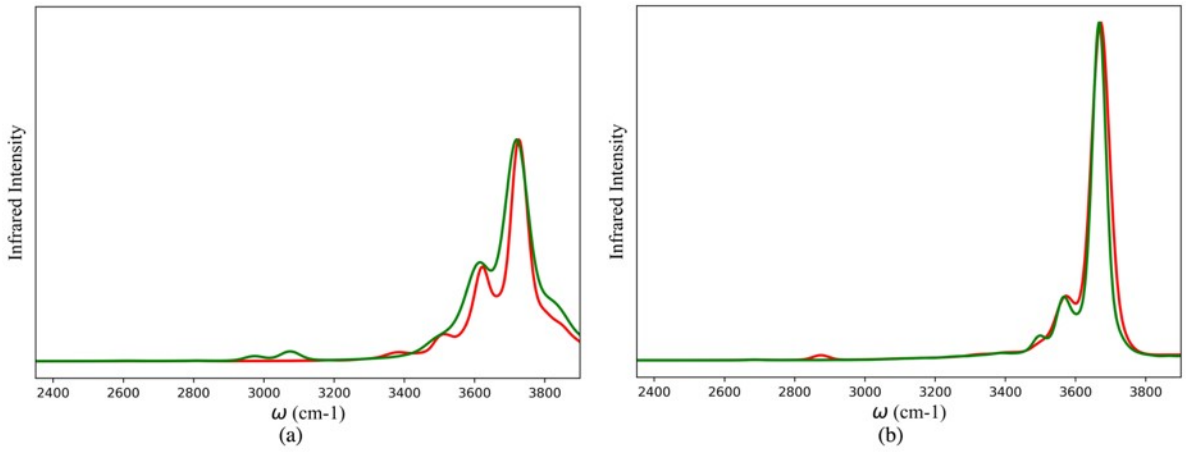

Figure S3: The theoretical IR spectra of water calculated with one water molecule locating at the (a) -NH_2 site in UiO-66-NH_2 and (b) -OH site in UiO-66-$(OH)_2$ with parameters from the General Amber Force Field (GAFF) (red line) or modified bond force field constants for N-H and O-H bonds on the organic linkers (green line).

To ensure that the bonded force field parameters in our force field can successfully reproduce the properties of the MOFs, we have benchmarked them against experimental infrared spectroscopic data.[4–7] The force field parameters for the functionalized linkers were extracted from the GAFF database.[2] It is therefore important to test their validity for modelling the functionalised MOFs. In the case of UiO-66-NH_2 (Figure S3a), the ν_s and ν_{as} of N-H arise at 2975 and 3079 cm^{-1} when the GAFF force field parameters[2] are used. Both of these computed frequencies are lower than those detected in the experimental IR spectrum of this MOF (ν_s = 3397 cm^{-1}, ν_{as} = 3514 cm^{-1}).[4,7] Thus, we adjusted the N-H bond force field parameters based on the experimental N-H vibrational frequency[4,7] using the following expression:

$$\frac{\nu_{calc}}{\sqrt{k_{GAFF}}} = \frac{\nu_{exp}}{\sqrt{k_{derived}}} \quad (1)$$

This expression was derived based on Hooke's law, where ν_{calc} is the vibrational frequency calculated using the N-H bond force field parameters from GAFF (k_{GAFF}).[2] Using this equation and the vibrational frequencies for N-H from the experimental spectra (ν_{exp}) we can derive the adjusted N-H force constant ($k_{derived}$). The IR spectrum calculated with $k_{derived}$ features ν_s at 3372 cm^{-1} and ν_{as} at 3496 cm^{-1} (Figure S3a), which is consistent with the experimental IR spectra.[4,7] Similarly, the vibration of the O-H groups on the linkers in UiO-66-OH and UiO-66-$(OH)_2$ calculated using the GAFF bonded force field parameters[2] (Figure S3b) appears at lower frequencies (2875 cm^{-1}) compared to experimental studies (3400-3500 cm^{-1}).[4–6] After adjusting the bonded force field parameters according to Eq (1) the O-H stretching shifted to 3499 cm^{-1}. Overall, the comparison between computed and experimental IR spectra allowed us to improve the parametrisation of the force field for the functionalized MOFs.[4–7]

2. Non-bonded force field parameter derivation and benchmark

2.1. Cluster models for density functional theory calculations

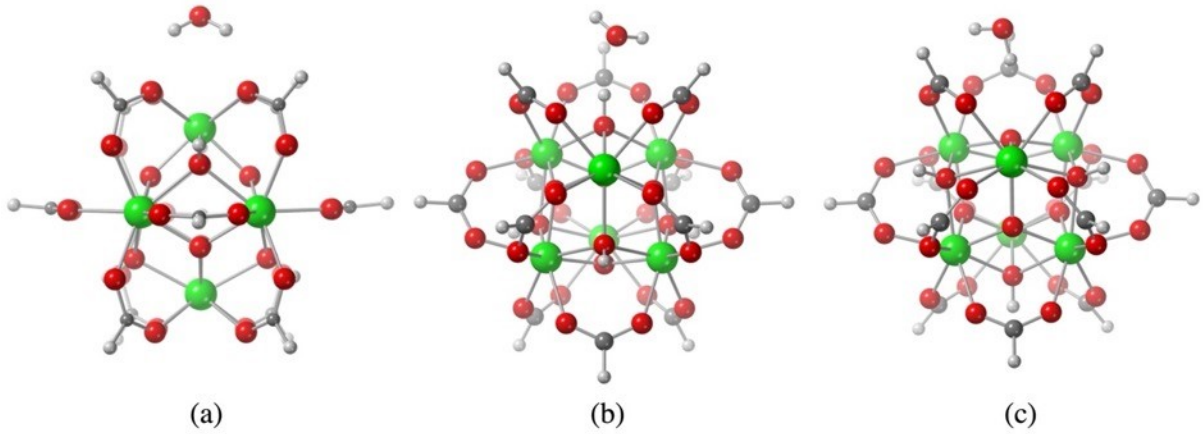

Figure S4: The optimised geometry of water interacting with the (a) O_{linker}, (b) μ_3-OH and (c) μ_3-O sites in UiO-66 with unconstrained UiO-66 cluster atoms. Zr atoms are represented by green spheres, O atoms by red spheres, C atoms by grey spheres, and H atoms by white spheres.

2.2. Benchmarking non-bonded force field parameters

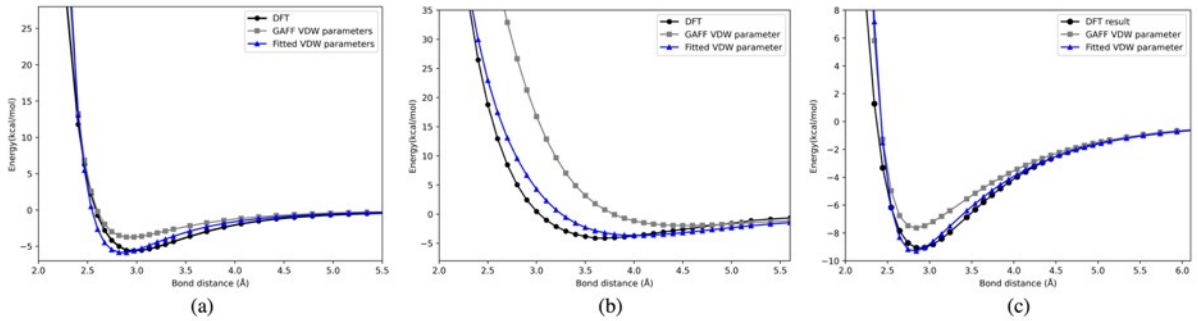

Figure S5: Comparison of the water and (a) O_{linker}, (b) μ_3-O, and (c) μ_3-OH interaction energy curves calculated with different approaches: (i) density functional theory (black curve); (ii) force field using non-bonded parameters from Universal Force Field (UFF) for Zr atoms and General Amber Force Fields (GAFF) for all other atoms with Lorentz-Berthelot mixing rules for the interaction between different atom types (grey curve); (iii) this same force field ad hoc developed Buckingham parameters for the HW···O_{linker}, HW···μ_3-O and OW···μ_3-OH interactions (blue curve).

Figure S5 compares the performance of the force field with non-bonded parameters fully derived from existing General Amber Force Fields (GAFF)[2] and Universal Force Field (UFF)[3] databases and the force field including the newly developed HW···O_{linker}, HW···μ_3-O and OW···μ_3-OH Buckingham parameters at reproducing the DFT PESs for the MOF-water interaction. The PESs calculated with the force field including the newly developed Buckingham parameters show good agreement with the DFT results, especially in the region close to the potential well, which is where the water is at the equilibrium distance from the interaction sites on the MOF. Ultimately, this indicates that the modified force field with the newly developed VDW parameters can successfully reproduce the interaction energies between water and the O_{linker}, μ_3-O, and μ_3-OH sites.

3. Simulation of different water loadings

In Figure 1a of the main text we show the experimental adsorption isotherm for UiO-66 as well as the number of water molecules included in the simulation cell of the UiO-66 MOF to represent different relative humidity (RH) levels. These numbers were derived based on the weight percentage (wt%) of water reported in the experimental adsorption isotherm.[8] The mass of water (m_{water}) in a 1 x 1 x 1 unit cell of the MOF can be calculated using the mass of the unit cell (m_{MOF}) model:

$$m_{water} = wt\%\ of\ water\ in\ MOF \times m_{MOF} \quad (2)$$

The number of water molecules (n_{water}) in the unit cell of MOF can be therefore determined using the molecular mass of water (M_{water}):

$$n_{water} = \frac{m_{water}}{M_{water}} \quad (3)$$

4. Deuterium labeling for IR peak assignment

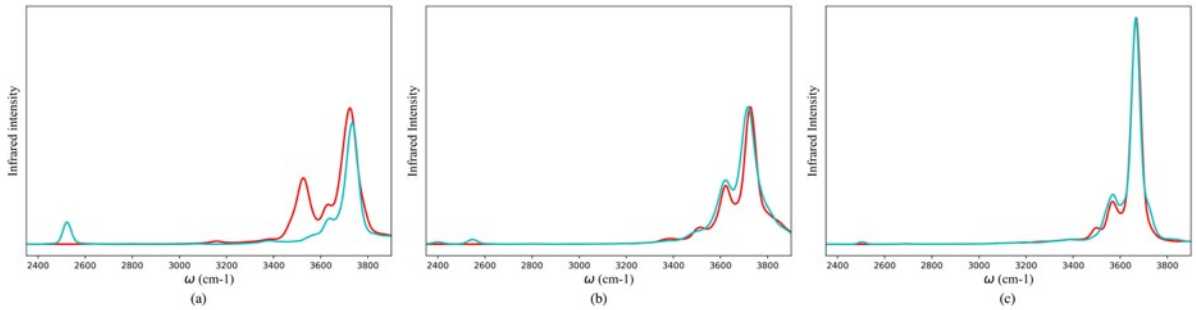

Figure S6: The theoretical IR spectra of water calculated with one water molecule locating at the (a) μ_3-OH site in UiO-66, (b) -NH_2 site in UiO-66-NH_2 and (c) -OH site in UiO-66-$(OH)_2$ with (green line) and without (red line) labelling the hydrogen (H) atom as deuterium (D) on the interaction sites.

We have assigned the peaks in the 3400-3500 cm^{-1} region of the IR spectra of water in the MOFs (see Figure 4, 6, and 7 in the main text) to the O-H stretch of water induced by the vibration of the framework interaction sites. This assignment was performed by labeling the H atoms of the μ_3-OH, -NH_2, and -OH groups with deuterium (D) to unequivocally determine the IR signals of water induced by the vibration of the corresponding interaction sites (Figure S6). When replacing the interested hydrogen atoms with D atoms, we expect to see a red-shift of the vibrational frequency of water if the O-H stretch signal of water is induced by the vibration of the functional group of interest. We have found that the O-H stretch coupled to the vibration of μ_3-OD and -OD appears around 2500 cm^{-1} (Figure S6a and c). While for -ND_2, two peaks arise around 2400 and 2500 cm^{-1} corresponding to the O-H stretch of water coupled to the $\nu_s$and ν_{as}stretch of -ND_2 group (Figure S6b). Thus, we have confirmed that the signal at 3400-3500 cm^{-1} region is due to the O-H stretch of water induced by the vibration of the framework interaction sites.

5. Additional radial distribution functions

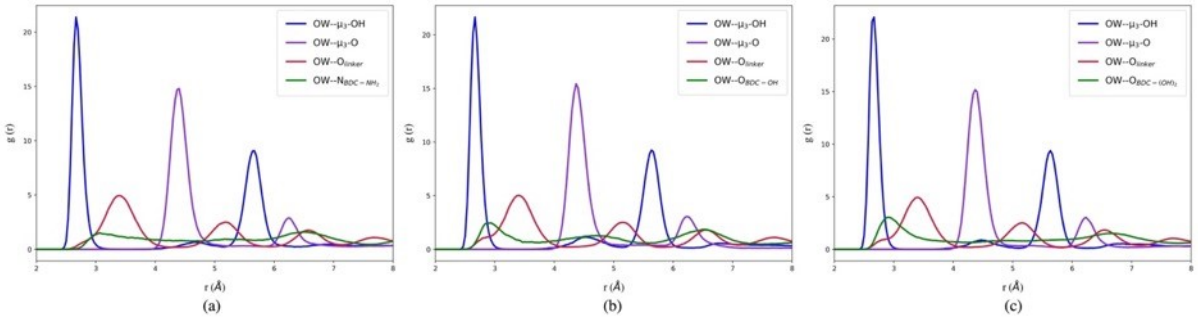

Figure S7: The radial distribution function (RDF) between the oxygen of water (OW) and the oxygen or nitrogen atoms in the μ_3-OH, μ_3-O, O_{linker}, -OH and -NH_2 interaction sites in (a) UiO-66-NH_2, (b) -OH, and (c) –$(OH)_2$. All plots were obtained from simulations with the same number of water molecules per unit cell as UiO-66 at 10% relative humidity (RH).

In the main text (Figures 2) we have shown the radial distribution functions (RDFs) between the oxygen (OW) of water and the oxygen and nitrogen atoms of the functional groups. For the sake of completion, in Figure S7 we show the RDFs between OW and all the interaction sites available in the functionalized MOFs (namely, μ_3-OH, μ_3-O, O_{linker}, -OH, and -NH_2). These plots show that the RDFs between OW and the μ_3-OH, μ_3-O, and O_{linker} sites peak at similar distances as the RDFs for water in UiO-66.

6. Additional two-dimensional density distribution maps

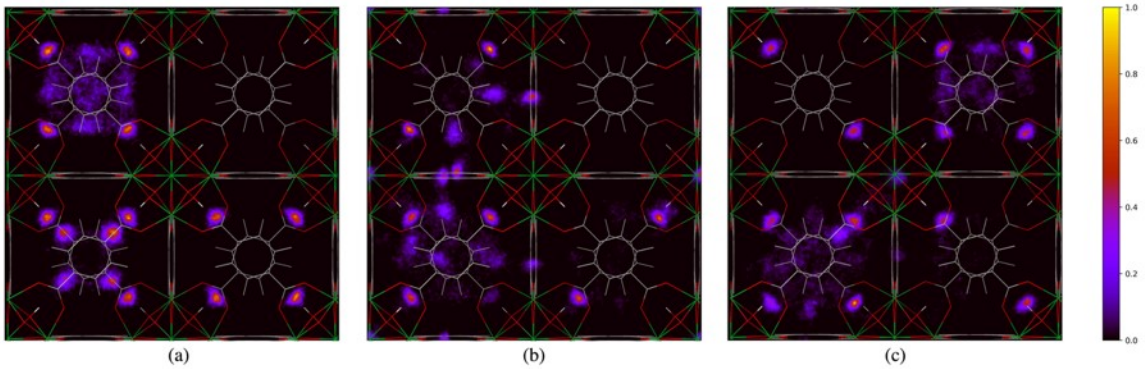

Figure S8: Two-dimensional density distribution maps calculated from single trajectories for water within UiO-66 at 20% relative humidity (RH) along the xy-plane. Refer to Figure 1b to identify the position of the different pores and relevant interaction sites in the density maps. The scale bar indicates the density of water relative to the highest density region in the unit cell.

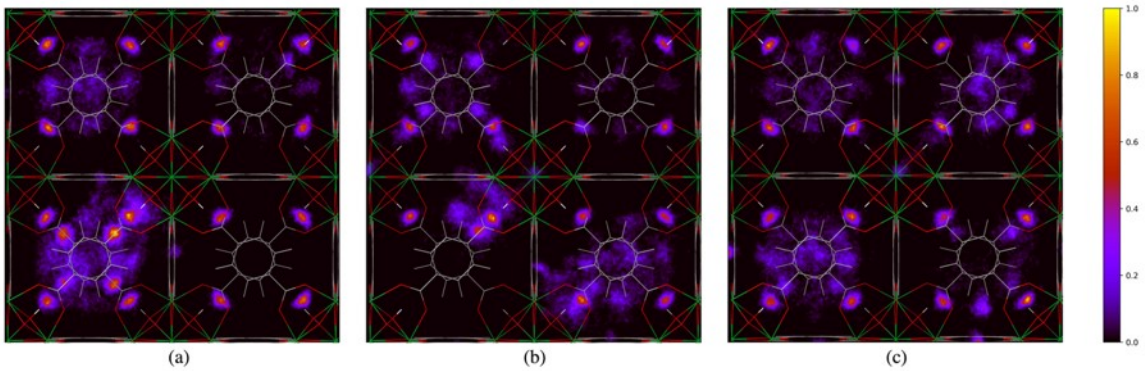

Figure S9: Two-dimensional density distribution maps calculated from single trajectories for water within UiO-66 at 30% relative humidity (RH) along the xy-plane. Refer to Figure 1b to identify the position of the different

pores and relevant interaction sites in the density maps. The scale bar indicates the density of water relative to the highest density region in the unit cell.

The density distribution maps of water calculated from single trajectories show water molecules preferentially interacting with each other in the tetrahedral pores and forming water clusters around the μ_3-OH sites at 20% RH rather than distributing evenly across all tetrahedral pores (Figure S8). At 30% RH, the majority of the water molecules are still located in the tetrahedral pores but they achieve a relatively more even distribution across these pores compared to 20% RH by diffusing through the octahedral pores to reach neighbouring tetrahedral pores.

7. Periodic DFT convergence tests

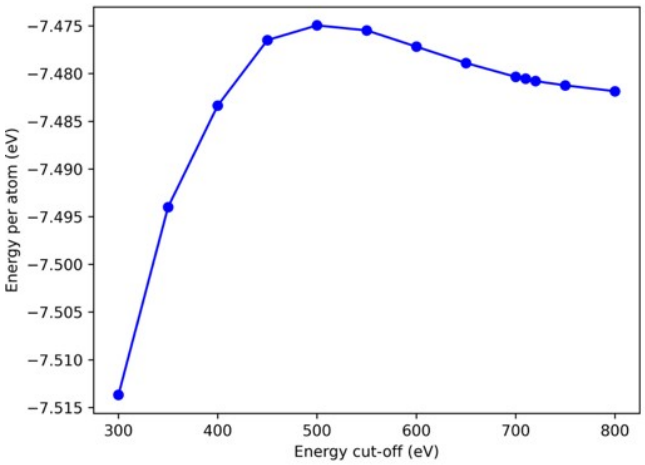

Figure S10: The energy per atom of the UiO-66 primitive unit cell calculated with different energy cut-off value and a 2 × 2 × 2 k-point mesh.

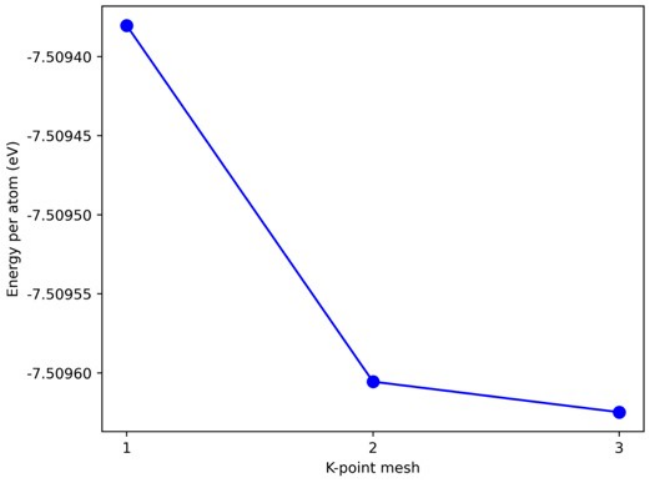

Figure S11: The energy per atom of the UiO-66 primitive unit cell calculated with different k-point mesh values and 700 eV energy cut-off.

The energy convergence diagrams generated with different energy cut-off and k-point meshes demonstrate that the energy is well converged with the energy cut-off (700 eV) and k-point mesh (2 × 2 × 2) used to optimize the unit cell of UiO-66 with periodic DFT calculations.

8. Force field parameters

8.1 Definition of atom types

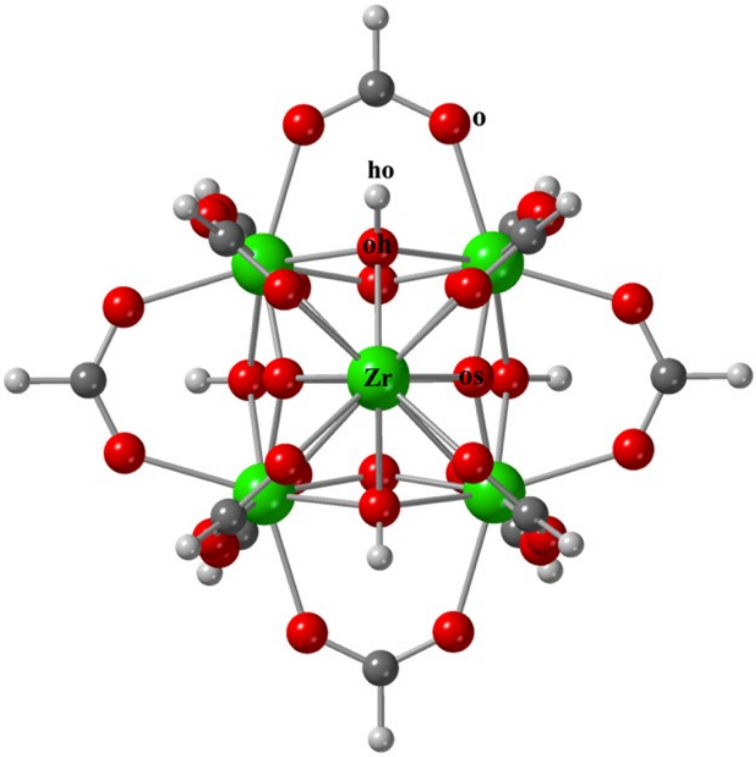

Figure S12: Force field atom types defined for the Zr oxide secondary building units (SBUs) of the functionalized and unfunctionalized UiO-66 MOFs. Zr atoms are represented by green spheres, O atoms by red spheres, C atoms by grey spheres, and H atoms by white spheres.

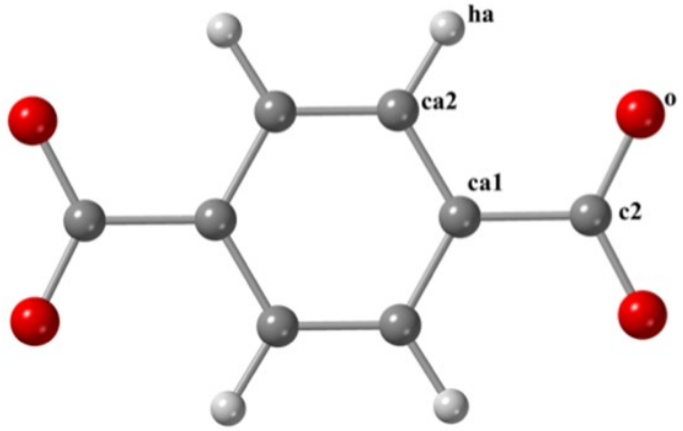

Figure S13: Force field atom types defined for the BDC organic linkers in UiO-66. O atoms are represented by red spheres, C atoms by grey spheres, and H atoms by white spheres.

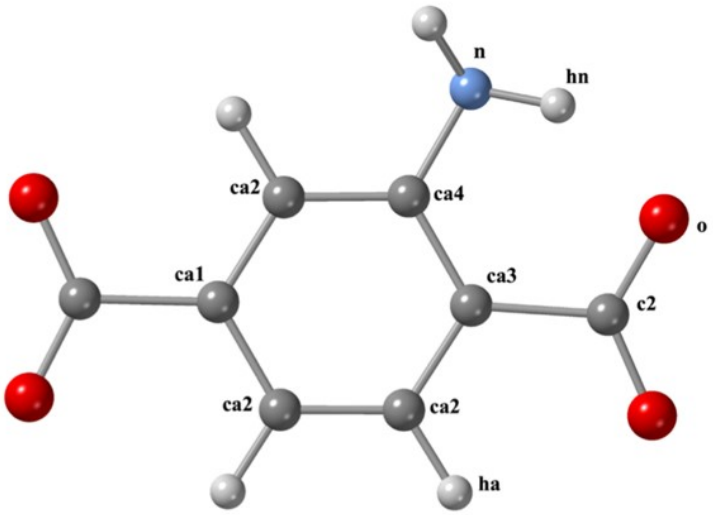

Figure S14: Force field atom types defined for the BDC-NH_2 organic linkers in UiO-66-NH_2. O atoms are represented by red spheres, C atoms by grey spheres, H atoms by white spheres, and N atom by blue sphere.

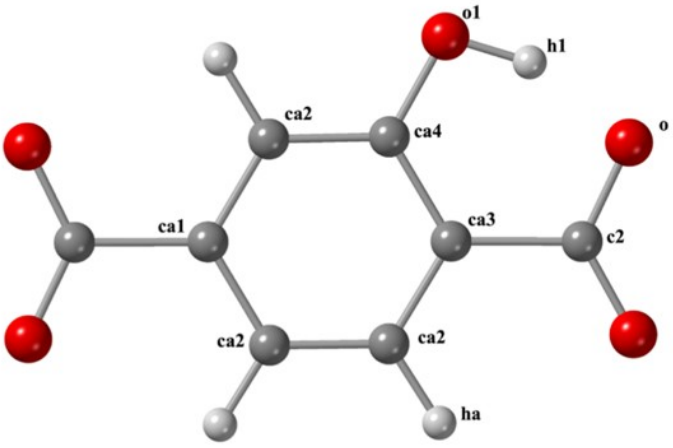

Figure S15: Force field atom types defined for the BDC-OH organic linkers in UiO-66-OH. O atoms are represented by red spheres, C atoms by grey spheres, and H atoms by white spheres.

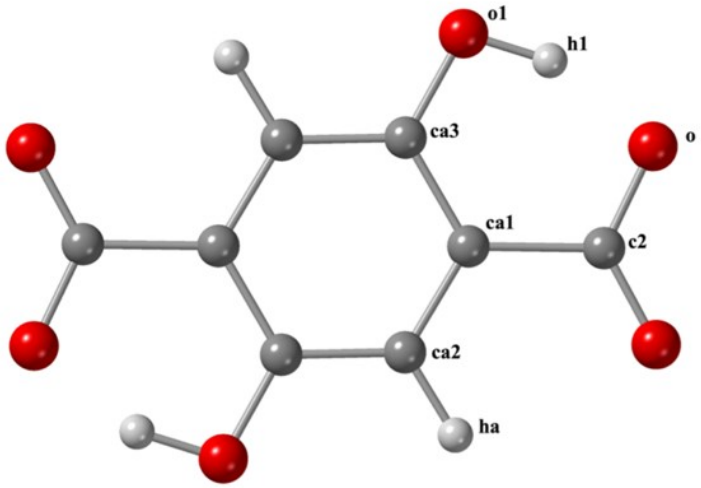

Figure S16: Force field atom types used for the BDC-$(OH)_2$ organic linkers in UiO-66-$(OH)_2$. O atoms are represented by red spheres, C atoms by grey spheres, and H atoms by white spheres.

8.2 Non-bonded force field parameters

Table S2: The derived Buckingham potential for HW···O_{linker} and HW···μ_3-O and OW···μ_3-OH interactions. $U(r) = Aexp\left(-\frac{r_{ij}}{\rho}\right) - \frac{C}{r_{ij}^6}$

Atom 1	Atom 2	A (kcal·mol^{-1})	ρ (Å)	C (Å^{-6})
HW	o	13578.847	0.204	82.864
HW	os	92390.864	0.206	973.552
OW	ho	12208.988	0.206	76.587

Table S3: The electrostatic and Lennard-Jones potentials for atoms in UiO-66. $U(r) = 4\epsilon\left[\left(\frac{\sigma}{r}\right)^{12} - \left(\frac{\sigma}{r}\right)^{6}\right]$

Atom names	Atom types	Charges	ϵ (kcal·mol^{-1})	$\sigma/2$ (Å)
Zr	Zr	1.616	0.069	1.392
c2	c2	0.196	0.086	1.700
o	o	-0.339	0.210	1.480
os	os	-0.762	0.210	1.480
oh	oh	-0.653	0.210	1.480
ca1	ca	-0.010	0.086	1.700
ca2	ca	-0.090	0.086	1.700
ha	ha	0.104	0.015	1.300
ho	ho	0.386	0	0

Table S4: The electrostatic and Lennard-Jones potentials for atoms in UiO-66-NH_2. $U(r) = 4\epsilon\left[\left(\frac{\sigma}{r}\right)^{12} - \left(\frac{\sigma}{r}\right)^{6}\right]$

Atom names	Atom types	Charges	ϵ (kcal·mol^{-1})	$\sigma/2$ (Å)
Zr	Zr	1.615	0.069	1.392
c2	c2	0.201	0.086	1.700
o	o	-0.340	0.210	1.480
os	os	-0.764	0.210	1.480
oh	oh	-0.654	0.210	1.480
ca1	ca	-0.008	0.086	1.700
ca2	ca	-0.103	0.086	1.700
ca3	ca	-0.028	0.086	1.700
ca4	ca	0.109	0.086	1.700
n	n	-0.636	0.170	1.625
hn	hn	0.297	0.016	0.535
ha	ha	0.102	0.015	1.300
ho	ho	0.385	0	0

Table S5: The electrostatic and Lennard-Jones potentials for atoms in UiO-66-OH. $U(r) = 4\epsilon\left[\left(\frac{\sigma}{r}\right)^{12} - \left(\frac{\sigma}{r}\right)^{6}\right]$

Atom names	Atom types	Charges	ϵ (kcal·mol^{-1})	$\sigma/2$ (Å)
Zr	Zr	1.618	0.069	1.392
c2	c2	0.208	0.086	1.700
o	o	-0.337	0.210	1.480
os	os	-0.760	0.210	1.480
oh	oh	-0.651	0.210	1.480
ca1	ca	-0.001	0.086	1.700
ca2	ca	-0.100	0.086	1.700
ca3	ca	-0.037	0.086	1.700
ca4	ca	0.106	0.086	1.700
o1	o1	-0.415	0.210	1.533
ha	ha	0.108	0.015	1.300
h1	h1	0.318	0	0
ho	ho	0.385	0	0

Table S6: The electrostatic and Lennard-Jones potentials for atoms in UiO-66-$(OH)_2$. $U(r) = 4\epsilon\left[\left(\frac{\sigma}{r}\right)^{12} - \left(\frac{\sigma}{r}\right)^{6}\right]$

Atom names	Atom types	Charges	ϵ (kcal·mol^{-1})	$\sigma/2$ (Å)
Zr	Zr	1.620	0.069	1.392
c2	c2	0.210	0.086	1.700
o	o	-0.335	0.210	1.480
os	os	-0.758	0.210	1.480
oh	oh	-0.649	0.210	1.480
ca1	ca	-0.024	0.086	1.700
ca2	ca	-0.097	0.086	1.700
ca3	ca	-0.090	0.086	1.700
o1	o1	-0.424	0.210	1.533
ha	ha	0.116	0.015	1.300
h1	h1	0.318	0	0
ho	ho	0.390	0	0

8.3 Bonded force field parameters

Table S7: The force field parameters for the bond potentials of the UiO-66 metal node. $U(r) = \frac{1}{2}k_b(r - r_0)^2$

Bond type (harmonic)	k_b (kcal·mol^{-1}· Å^{-2})	r_0 (Å)
Zr-oh	222.028	1.928
Zr-o	920.000	2.214
Zr-os	172.237	2.086
oh-ho	1079.572	0.973

Table S8: The force field parameters for the bond potentials of the BDC organic linker. $U(r) = \frac{1}{2}k_b(r - r_0)^2$

Bond type (harmonic)	k_b (kcal·mol^{-1}· Å^{-2})	r_0 (Å)
c2-o	1275.400	1.218
c2-ca	691.800	1.491
ca-ca	922.200	1.398
ca-ha	691.600	1.086

Table S9: The force field parameters for the bond potentials of the BDC-NH_2 organic linkers. $U(r) = \frac{1}{2}k_b(r - r_0)^2$

Bond type (harmonic)	k_b (kcal·mol^{-1}· Å^{-2})	r_0 (Å)
c2-o	1275.400	1.218
c2-ca	691.800	1.491
ca-ca	922.200	1.398

ca-ha	691.600	1.086
ca-n	835.800	1.386
hn-n	1105.534	1.012

Table S10: The force field parameters for the bond potentials of the BDC-OH organic linkers. $U(r) = \frac{1}{2}k_b(r - r_0)^2$

Bond type (harmonic)	k_b (kcal·mol^{-1}· Å^{-2})	r_0 (Å)
c2-o	1275.400	1.218
c2-ca	691.800	1.491
ca-ca	922.200	1.398
ca-ha	691.600	1.086
ca-o1	768.000	1.364
o1-h1	1079.572	0.973

Table S11: The force field parameters for the bond potentials of the BDC-$(OH)_2$ organic linkers. $U(r) = \frac{1}{2}k_b(r - r_0)^2$

Bond type (harmonic)	k_b (kcal·mol^{-1}· Å^{-2})	r_0 (Å)
c2-o	1275.400	1.218
c2-ca	691.800	1.491
ca-ca	922.200	1.398
ca-ha	691.600	1.086
ca-o1	768.000	1.364
o1-h1	1079.572	0.973

Table S12: The force field parameters for the bending potentials of the UiO-66 metal node. $U(\theta) = \frac{1}{2}k_a(\theta - \theta_0)^2$

Bond type (harmonic)	k_a (kcal·mol^{-1})	θ_0
Zr-os-Zr	70.457	114.287
Zr-oh-Zr	69.298	109.647
Zr-oh-ho	123.716	100.027
Zr-o-c2	140.533	127.251
os-Zr-o	22.696	104.677
os-Zr-oh	104.430	59.098
os-Zr-os	72.303	87.027
oh-Zr-oh	141.846	98.835
oh-Zr-o	88.596	92.633
o-Zr-o	26.751	73.527

Table S13: The force field parameters for the bending potentials of the BDC organic linker. $U(\theta) = \frac{1}{2}k_a(\theta - \theta_0)^2$

Bond type (harmonic)	k_a (kcal·mol^{-1})	θ_0
o-c2-o	155.800	130.250
o-c2-ca	137.400	122.600
c2-ca-ca	128.600	120.330
ca-ca-ha	96.400	119.880
ca-ca-ca	133.200	120.020

Table S14: The force field parameters for the bending potentials of BDC-NH_2 organic linkers. $U(\theta) = \frac{1}{2}k_a(\theta - \theta_0)^2$

Bond type (harmonic)	k_a (kcal·mol^{-1})	θ_0
o-c2-o	155.800	130.250
o-c2-ca	137.400	122.600
c2-ca-ca	128.600	120.330
ca-ca-ha	96.400	119.880
ca-ca-ca	133.200	120.020
ca-ca-n	136.600	120.950
ca-n-hn	96.800	116.070
hn-n-hn	80.200	115.120

Table S15: The force field parameters for the bending potentials of BDC-OH organic linkers. $U(\theta) = \frac{1}{2}k_a(\theta - \theta_0)^2$

Bond type (harmonic)	k_a (kcal·mol^{-1})	θ_0
o-c2-o	155.800	130.250
o-c2-ca	137.400	122.600
c2-ca-ca	128.600	120.330
ca-ca-ha	96.400	119.880
ca-ca-ca	133.200	120.020
ca-ca-o1	139.000	119.900
ca-o1-h1	98.000	108.580

Table S16: The force field parameters for the bending potentials of BDC-$(OH)_2$ organic linkers. $U(\theta) = \frac{1}{2}k_a(\theta - \theta_0)^2$

Bond type (harmonic)	k_a (kcal·mol^{-1})	θ_0
o-c2-o	155.800	130.250

o-c2-ca	137.400	122.600
c2-ca-ca	128.600	120.330
ca-ca-ha	96.400	119.880
ca-ca-ca	133.200	120.020
ca-ca-o1	139.000	119.900
ca-o1-h1	98.000	108.580

Table S17: The force field parameters for the dihedral angle potentials of the BDC organic linkers. $U(\phi(ijkn)) = A[1 + \cos(m\phi_{ijkn} - \delta)]$

Dihedral type	A (kcal·mol^{-1})	δ	m
ha-ca-ca-ha	3.625	180.000	2
ca-ca-ca-ca	3.625	180.000	2
ca-ca-ca-ha	3.625	180.000	2
ha-ca-ca-c2	3.625	180.000	2
ca-ca-ca-c2	3.625	180.000	2
ca-ca-c2-o	1.100	180.000	2

Table S18: The force field parameters for the dihedral angle potentials of the BDC-NH_2 organic linkers. $U(\phi(ijkn)) = A[1 + \cos(m\phi_{ijkn} - \delta)]$

Dihedral type	A (kcal·mol^{-1})	δ	m
ha-ca-ca-ha	3.625	180.000	2
ca-ca-ca-ca	3.625	180.000	2
ca-ca-ca-ha	3.625	180.000	2
ha-ca-ca-c2	3.625	180.000	2
ca-ca-ca-c2	3.625	180.000	2
ca-ca-c2-o	1.100	180.000	2
c2-ca-ca-n	3.625	180.000	2
ca-ca-ca-n	3.625	180.000	2
ca-ca-n-hn	3.625	180.000	2
ha-ca-ca-n	3.625	180.000	2

Table S19: The force field parameters for the dihedral angle potentials of BDC-OH linkers. $U(\phi(ijkn)) = A[1 + \cos(m\phi_{ijkn} - \delta)]$

Dihedral type	A (kcal·mol^{-1})	δ	m
ha-ca-ca-ha	3.625	180.000	2
ca-ca-ca-ca	3.625	180.000	2
ca-ca-ca-ha	3.625	180.000	2
ha-ca-ca-c2	3.625	180.000	2
ca-ca-ca-c2	3.625	180.000	2
ca-ca-c2-o	1.100	180.000	2
c2-ca-ca-o1	3.625	180.000	2
ca-ca-ca-o1	3.625	180.000	2

ca-ca-o1-h1	0.900	180.000	2
ha-ca-ca-o1	3.625	180.000	2

Table S20: The force field parameters for the dihedral angle potentials of the BDC-$(OH)_2$ organic linkers. $U(\phi(ijkn)) = A[1 + \cos(m\phi_{ijkn} - \delta)]$

Dihedral type	A (kcal·mol^{-1})	δ	m
ca-ca-ca-ca	3.625	180.000	2
ca-ca-ca-ha	3.625	180.000	2
ha-ca-ca-c2	3.625	180.000	2
ca-ca-ca-c2	3.625	180.000	2
ca-ca-c2-o	1.100	180.000	2
c2-ca-ca-o1	3.625	180.000	2
ca-ca-ca-o1	3.625	180.000	2
ca-ca-o1-h1	0.900	180.000	2
ha-ca-ca-o1	3.625	180.000	2

Table S21: The force field parameters for the improper angle potentials of the BDC organic linkers. $U(\phi(ijkn)) = A[1 + \cos(m\phi_{ijkn} - \delta)]$

Dihedral type	A (kcal·mol^{-1})	δ	m
c2-ca-o-o	1.100	180.000	2
ca-ca-ca-ha	1.100	180.000	2
ca-c2-ca-ca	1.100	180.000	2

Table S22: The force field parameters for the improper angle potentials of the BDC-NH_2 organic linkers. $U(\phi(ijkn)) = A[1 + \cos(m\phi_{ijkn} - \delta)]$

Dihedral type	A (kcal·mol^{-1})	δ	m
c2-ca-o-o	1.100	180.000	2
ca-ca-ca-ha	1.100	180.000	2
ca-c2-ca-ca	1.100	180.000	2
ca-ca-ca-n	1.100	180.000	2
n-ca-hn-hn	1.100	180.000	2

Table S23: The force field parameters for the improper angle potentials of the BDC-OH organic linkers. $U(\phi(ijkn)) = A[1 + \cos(m\phi_{ijkn} - \delta)]$

Dihedral type	A (kcal·mol^{-1})	δ	m
c2-ca-o-o	1.100	180.000	2
ca-ca-ca-ha	1.100	180.000	2
ca-c2-ca-ca	1.100	180.000	2
ca-ca-ca-o1	1.100	180.000	2

Table S24: The force field parameters for the improper angle potentials of the BDC-$(OH)_2$ organic linkers. $U(\phi(ijkn)) = A[1 + \cos(m\phi_{ijkn} - \delta)]$

Dihedral type	A (kcal·mol^{-1})	δ	m
c2-ca-o-o	10.500	180.000	2
ca-ca-ca-ha	1.100	180.000	2
ca-c2-ca-ca	1.100	180.000	2
ca-ca-ca-o1	1.100	180.000	2

References

(1) Øien, S.; Wragg, D.; Reinsch, H.; Svelle, S.; Bordiga, S.; Lamberti, C.; Lillerud, K. P. Detailed Structure Analysis of Atomic Positions and Defects in Zirconium Metal-Organic Frameworks. *Cryst Growth Des* **2014**, *14* (11), 5370–5372. https://doi.org/10.1021/cg501386j.

(2) Wang, J.; Wang, W.; Kollman, P. A.; Case, D. A. Automatic Atom Type and Bond Type Perception in Molecular Mechanical Calculations. *J Mol Graph Model* **2006**, *25* (2). https://doi.org/10.1016/j.jmgm.2005.12.005.

(3) Rappé, A. K.; Casewit, C. J.; Colwell, K. S.; Goddard, W. A.; Skiff, W. M. UFF, a Full Periodic Table Force Field for Molecular Mechanics and Molecular Dynamics Simulations. *J Am Chem Soc* **1992**, *114* (25), 10024–10035. https://doi.org/10.1021/ja00051a040.

(4) Hadjiivanov, K. I.; Panayotov, D. A.; Mihaylov, M. Y.; Ivanova, E. Z.; Chakarova, K. K.; Andonova, S. M.; Drenchev, N. L. Power of Infrared and Raman Spectroscopies to Characterize Metal-Organic Frameworks and Investigate Their Interaction with Guest Molecules. *Chemical Reviews*. American Chemical Society February 10, 2021, pp 1286–1424. https://doi.org/10.1021/acs.chemrev.0c00487.

(5) Rada, Z. H.; Abid, H. R.; Shang, J.; Sun, H.; He, Y.; Webley, P.; Liu, S.; Wang, S. Functionalized UiO-66 by Single and Binary $(OH)_2$ and NO_2 Groups for Uptake of CO_2 and CH_4. *Ind Eng Chem Res* **2016**, *55* (29), 7924–7932. https://doi.org/10.1021/acs.iecr.5b04061.

(6) Moghaddam, Z. S.; Kaykhaii, M.; Khajeh, M.; Oveisi, A. R. Synthesis of UiO-66-OH Zirconium Metal-Organic Framework and Its Application for Selective Extraction and Trace Determination of Thorium in Water Samples by Spectrophotometry. *Spectrochim Acta A Mol Biomol Spectrosc* **2018**, *194*, 76–82. https://doi.org/10.1016/j.saa.2018.01.010.

(7) Veisi, H.; Abrifam, M.; Kamangar, S. A.; Pirhayati, M.; Saremi, S. G.; Noroozi, M.; Tamoradi, T.; Karmakar, B. Pd Immobilization Biguanidine Modified Zr-UiO-66 MOF as a Reusable Heterogeneous Catalyst in Suzuki–Miyaura Coupling. *Sci Rep* **2021**, *11* (1), 21883. https://doi.org/10.1038/s41598-021-00991-3.

(8) Furukawa, H.; Gándara, F.; Zhang, Y. B.; Jiang, J.; Queen, W. L.; Hudson, M. R.; Yaghi, O. M. Water Adsorption in Porous Metal-Organic Frameworks and Related

Materials. *J Am Chem Soc* **2014**, *136* (11), 4369–4381.
https://doi.org/10.1021/ja500330a.